

CuriGS: Curriculum-Guided Gaussian Splatting for Sparse View Synthesis

Zijian Wu

Zhejiang Sci-Tech University

2024110602006@mails.zstu.edu.cn

Mingfeng Jiang

Zhejiang Sci-Tech University

m.jiang@zstu.edu.cn

Zidian Lin

Zhejiang Sci-Tech University

2025010602002@mails.zstu.edu.cn

Ying Song

Zhejiang Sci-Tech University

ysong@zstu.edu.cn

Hanjie Ma

Zhejiang Sci-Tech University

mahanjie@zstu.edu.cn

Qun Wu

Zhejiang Sci-Tech University

wuq@zstu.edu.cn

Dongping Zhang

China Jiliang University

06a0303103@cjlu.edu.cn

Guiyang Pu

Zhejiang University

puguiyanghz@cmhi.chinamobile.com

Abstract

3D Gaussian Splatting (3DGS) has recently emerged as an efficient, high-fidelity representation for real-time scene reconstruction and rendering. However, extending 3DGS to sparse-view settings remains challenging because of supervision scarcity and overfitting caused by limited viewpoint coverage. In this paper, we present CuriGS, a curriculum-guided framework for sparse-view 3D reconstruction using 3DGS. CuriGS addresses the core challenge of sparse-view synthesis by introducing student views: pseudo-views sampled around ground-truth poses (teacher). For each teacher, we generate multiple groups of student views with different perturbation levels. During training, we follow a curriculum schedule that gradually unlocks higher perturbation level, randomly sampling candidate students from the active level to assist training. Each sampled student is regularized via depth-correlation and co-regularization, and evaluated using a multi-signal metric that combines SSIM, LPIPS, and an image-quality measure. For every teacher and perturbation level, we periodically retain the best-performing students and promote those that satisfy a predefined quality threshold to the training set, resulting in a stable augmentation of sparse training views. Experimental results show that CuriGS outperforms state-of-the-art baselines in both rendering fidelity and geometric consistency across various synthetic and real sparse-view scenes. Project page: <https://zijian1026.github.io/CuriGS/>

1. Introduction

In recent years, 3D reconstruction has advanced rapidly, becoming a key enabling technology in fields such as virtual reality, digital twins, cultural heritage preservation, and intelligent manufacturing [8, 29, 34, 45]. Among various approaches [25, 28, 38], Neural Radiance Fields (NeRF) [20] and its variants [3, 7, 24, 30] have achieved impressive results in high-fidelity reconstruction and photorealistic view synthesis using implicit volumetric representations, albeit with slow optimization and heavy computational costs. Recently, 3D Gaussian Splatting (3DGS) [13] has emerged as a more efficient and stable explicit representation, enabling real-time rendering by modeling scenes as point-based Gaussians with covariance, color, and opacity attributes [16, 18, 26, 32, 37, 39, 40, 46]. Beyond representation efficiency, sparse view synthesis [5, 6, 10, 17, 42] has become a key research focus, aiming to reconstruct accurate geometry and realistic appearance from only a few input images. This setting is both practical and highly challenging, as limited viewpoints lead to supervision scarcity and severe overfitting.

In response to these challenges, recent studies have explored various strategies for enhancing 3D reconstruction under sparse-input conditions. Within the NeRF family, SparseNeRF [36] introduces weak supervision by distilling depth-ordering priors, thereby constraining volumetric geometry and alleviating degradation under extremely limited viewpoints. FreeNeRF [43] approaches the problem from a frequency and occlusion regularization perspective, impos-

ing simple yet effective constraints on NeRF’s frequency spectrum and near-camera density distribution, which improves stability and generalization for few-shot rendering without external supervision.

In the context of 3DGS, FSGS [50] adapts 3DGS to sparse view synthesis through an efficient Gaussian expansion strategy, incorporating pretrained monocular depth estimation as a geometric prior to guide reconstruction. Similarly, DNGaussian [14] exploits depth information by employing a hard and soft depth-regularization scheme alongside a global-local depth-normalization strategy to reshape Gaussian primitives for more accurate geometry. Moreover, LoopSparseGS [2] proposes a loop-based framework that progressively densifies Gaussian initialization, aligns both scale-consistent and inconsistent depths for reliable geometry, and adopts sparse-aware sampling to mitigate oversized ellipsoid artifacts.

These studies address the challenge of sparse view reconstruction from different perspectives, proposing a variety of strategies to enhance reconstruction quality. In summary, their methods mainly rely on incorporating additional cues such as depth priors or introducing regularization mechanisms to alleviate overfitting. However, the fundamental limitation of sparse view reconstruction lies in the inherent lack of supervisory signals caused by extreme data sparsity, which restricts cross-view generalization and compromises geometric consistency. Consequently, while these methods offer partial improvements in visual quality, they do not fundamentally resolve the core issue. This persistent challenge drives our curriculum-based regularization framework, which aims to tackle the root cause of supervision deficiency rather than merely mitigating its symptoms.

Motivated by the above observations, we propose CuriGS, a curriculum-guided 3DGS framework designed for sparse view 3D reconstruction. The key idea of CuriGS is the introduction of student views—pseudo-views generated around real cameras (teacher) with controllable perturbation magnitudes. During training, a curriculum schedule progressively unlocks student groups with larger perturbations, allowing the model to gradually adapt from locally consistent to more diverse viewpoints. At each iteration, a subset of student views is randomly sampled from the currently active group and optimized through depth-correlation and co-regularization constraints, which enforce geometric consistency while mitigating reconstruction errors. Meanwhile, CuriGS maintains the best-performing student for each teacher and perturbation group, evaluated via a multi-signal metric combining structural similarity (SSIM), perceptual similarity (LPIPS), and a no-reference image-quality score [1]. Students that exceed a predefined quality threshold are periodically promoted into the training set, effectively augmenting sparse supervision with reliable pseudo-views. As illustrated in Fig. 1, this design ef-

fectively enriches the supervision signal under sparse-view conditions, improving both geometric fidelity and rendering realism while enhancing the model’s generalization to unseen viewpoints. The main contributions of this work are as follows:

1. Curriculum-guided sparse view expansion. We introduce the first curriculum-guided 3DGS framework that dynamically generates and promotes student views, expanding supervision directly from sparse inputs while mitigating overfitting and geometric inconsistency.
2. Unified pseudo-view learning mechanism. CuriGS provides a principled framework for generating, evaluating, and integrating pseudo-views into scene optimization, opening a new direction for virtual-view learning in reconstruction and synthesis tasks.
3. Superior performance and generalization. Extensive experiments across multiple benchmarks demonstrate that CuriGS consistently surpasses state-of-the-art baselines in rendering fidelity, perceptual quality, and geometric consistency.

2. Related Work

2.1. NeRF-based Sparse View Synthesis

While NeRF achieves photorealistic results under dense multi-view supervision, its optimization becomes severely ill-posed in sparse-view settings, often leading to geometry collapse, texture ambiguity, and overfitting to the observed views. To alleviate these issues, several methods [9, 11, 21, 30, 31, 36, 43] have been proposed to adapt NeRF-style representations for few-shot reconstruction.

SparseNeRF [36] introduces weak geometric supervision by distilling depth-ordering priors from pretrained monocular depth estimators or coarse sensor depth. By injecting such constraints into the volumetric optimization, SparseNeRF reduces geometric ambiguity and mitigates depth collapse when only a handful of views are available. However, its performance heavily depends on the quality and domain alignment of the external depth priors, which may mislead optimization when the monocular estimator is biased or out-of-domain. FreeNeRF [43] approaches the problem from a spectral and occlusion-regularization perspective, imposing frequency and near-camera density constraints on the learned radiance field to suppress unsupported high-frequency components and spurious near-field densities that commonly arise under sparse supervision. This family of regularizers is appealing for its simplicity and independence from explicit external priors, but it requires careful hyperparameter tuning and may attenuate genuine high-frequency surface details in richly textured scenes. PixelNeRF [44] extends NeRF into a conditional formulation by leveraging learned multi-view feature fusion. Through large-scale multi-scene pretraining,

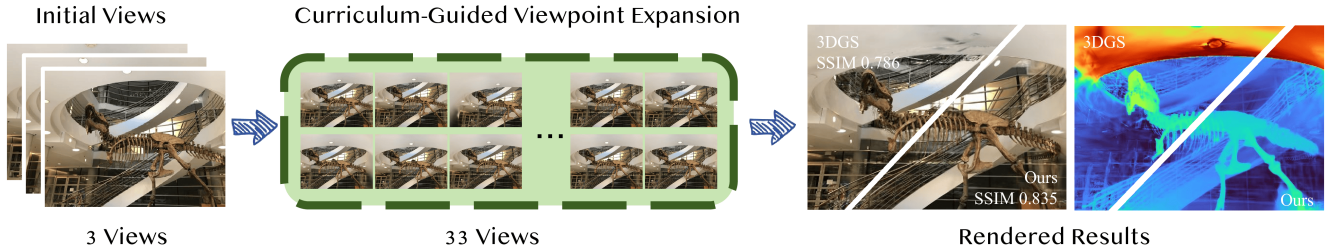


Figure 1. CuriGS is a curriculum-guided Gaussian Splatting framework that enhances sparse-view 3D reconstruction by progressively introducing pseudo-views with increasing perturbations, yielding stable geometry and photorealistic rendering from extremely limited input views.

it improves few-shot generalization and cross-scene adaptability, yet still struggles with limited fidelity and unstable geometry when applied to novel domains that diverge from the training distribution. Despite these advances, sparse-view NeRFs are fundamentally constrained by their implicit volumetric representation. Consequently, achieving stable geometry and consistent appearance reconstruction under extremely sparse inputs remains a significant challenge, motivating the development of alternative representations and training paradigms that can inherently cope with data scarcity.

2.2. 3DGS-based Sparse View Synthesis

Compared with NeRF, 3DGS offers superior runtime efficiency, interpretable geometric primitives, and direct manipulability, making it particularly appealing for interactive visualization and efficient optimization. Motivated by these strengths, several studies [14, 15, 22, 23, 47–50] have explored its potential for sparse view synthesis tasks with most achieving notably better performance than NeRF-based methods.

CoR-GS [47] introduces an ensemble-based strategy in which multiple 3DGS instances are trained jointly, using mutual inconsistencies in both point-level geometry and rendered appearance to identify and suppress unreliable splats through co-pruning. This co-regularization effectively reduces reconstruction artifacts without relying on explicit ground-truth geometry. However, the method increases training complexity and computational overhead, and its effectiveness diminishes in highly symmetric or extremely sparse scenes where ensemble disagreement becomes ambiguous. NexusGS [49] introduces an epipolar-depth-guided framework that integrates geometric priors to guide Gaussian densification, pruning, and blending. However, it relies on additional optical flow information and performs poorly when training views have low overlap, which limits its applicability. DropGaussian [23] proposes a lightweight structural regularization strategy by randomly deactivating subsets of Gaussians during training. This dropout-like mechanism redistributes gradients toward

under-optimized splats, mitigating overfitting and improving generalization to unseen views. Unlike methods that rely on external priors or ensemble models, DropGaussian is simple and computationally efficient, though its stochastic nature may lead to unstable convergence or suboptimal results in extremely sparse or unstructured scenes.

Beyond the representative works discussed above, other 3DGS-based sparse-view methods [2, 33, 35, 41] have made progress by incorporating semantic guidance, Gaussian super-resolution, or confidence-weighted sparse enhancements to stabilize optimization. Nevertheless, these approaches fundamentally build upon stronger regularization or auxiliary supervision and do not address the key challenge of sparse view reconstruction, namely the intrinsic scarcity of training viewpoints, thus remaining methodologically constrained. In contrast, we directly tackle the fundamental limitation of sparse training supervision by expanding the available viewpoints through a curriculum-guided pseudo-view learning strategy.

3. Method

In this section, we present CuriGS, a curriculum-guided, data-centric sparse-view 3DGS framework that progressively expands the effective training view distribution through the generation, evaluation, and selection of pseudo-views. The overall pipeline of the proposed method is illustrated in Fig. 2.

3.1. Preliminaries: Gaussian Splatting

3DGS represents a scene as a set of anisotropic Gaussian primitives, each parameterized by position $\mu \in \mathbb{R}^3$, covariance $\Sigma \in \mathbb{R}^{3 \times 3}$, opacity $\alpha \in [0, 1]$, and spherical harmonic (SH) coefficients for view-dependent color. Formally, each Gaussian defines a density function in 3D space:

$$G(\mathbf{x}) = \exp\left(-\frac{1}{2}(\mathbf{x} - \mu)^\top \Sigma^{-1}(\mathbf{x} - \mu)\right) \quad (1)$$

The rendering process follows a rasterization pipeline, in which each Gaussian is splatted into screen space, composited according to depth order, and accumulated using alpha

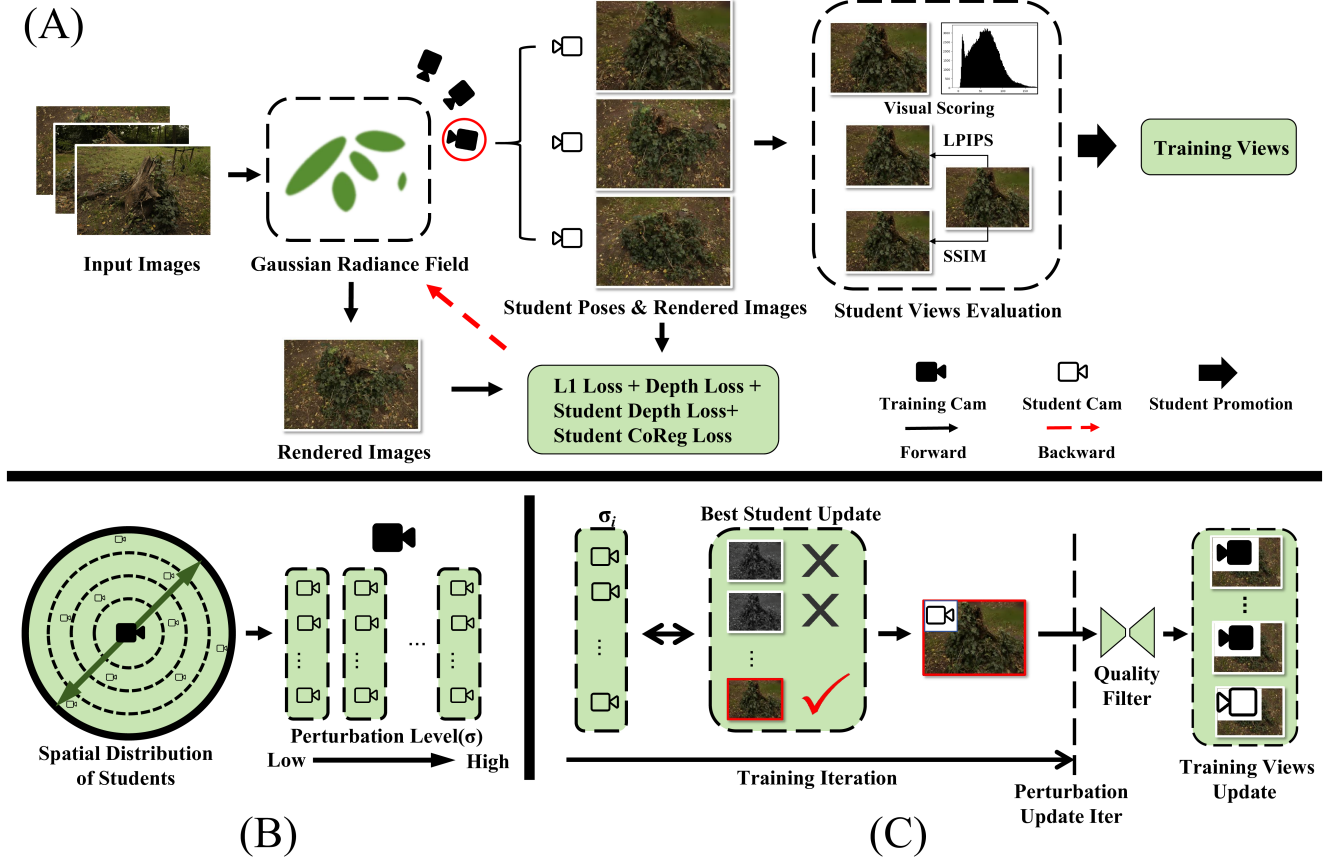


Figure 2. The overall architecture of the CuriGS framework is shown in (A). The pipeline consists of three key stages: (1) student view generation, where pseudo-camera poses are sampled around teacher views with multiple perturbation magnitudes, as detailed in (B); (2) curriculum scheduling, which gradually unlocks perturbation levels during training to progressively expand viewpoint diversity; and (3) student view evaluation and promotion, where each candidate is scored using perceptual (LPIPS), structural (SSIM), and no-reference quality metrics. Only the best student at each perturbation level that passes the evaluation criteria is promoted to the training set, as illustrated in (C). This curriculum-guided process enhances geometric consistency and rendering fidelity under sparse supervision.

blending. Specifically, the pixel color $C(\mathbf{p})$ at screen location \mathbf{p} is obtained by front-to-back alpha compositing:

$$C(\mathbf{p}) = \sum_{i=1}^N T_i \alpha_i \mathbf{c}_i(\mathbf{p}), \quad T_i = \prod_{j=1}^{i-1} (1 - \alpha_j), \quad (2)$$

where α_i denotes the opacity of the i -th Gaussian, $\mathbf{c}_i(\mathbf{p})$ is its color contribution, and T_i is the transmittance term accounting for accumulated transparency from closer Gaussians.

3.2. Curriculum: Student View Generation and Scheduling

Student view generation. The key idea of our framework is the introduction of student views with the goal of augmenting supervision by generating novel viewpoints that remain geometrically consistent with the original camera distribution, while progressively increasing diversity during

training. Specifically, we generate student views by perturbing the extrinsics of each teacher camera within a controlled range. Given a teacher camera with rotation R and translation T , we first calculate its optical center $C = -R^\top T$. Random angular perturbations in yaw and pitch are then applied, sampled from a zero-mean Gaussian distribution with a standard deviation σ (in degrees), together with a mild radial perturbation σ_r along the viewing direction, both of which collectively simulate small camera displacements.:

$$\begin{aligned} R' &= R R_\Delta(\sigma), & C' &= C(1 + \epsilon_r), & \epsilon_r &\sim \mathcal{N}(0, \sigma_r^2), \\ T' &= -R' C'. \end{aligned} \quad (3)$$

The perturbed parameters (R', T') define a new pseudo-view centered near the teacher pose and preserving identical intrinsic calibration.

For each teacher view C_t , we initialize multiple groups of student views $\mathcal{P}(\sigma_i) = \{C_s^{\sigma_i, j}\}_{j=1}^{N_i}$ with varying angular

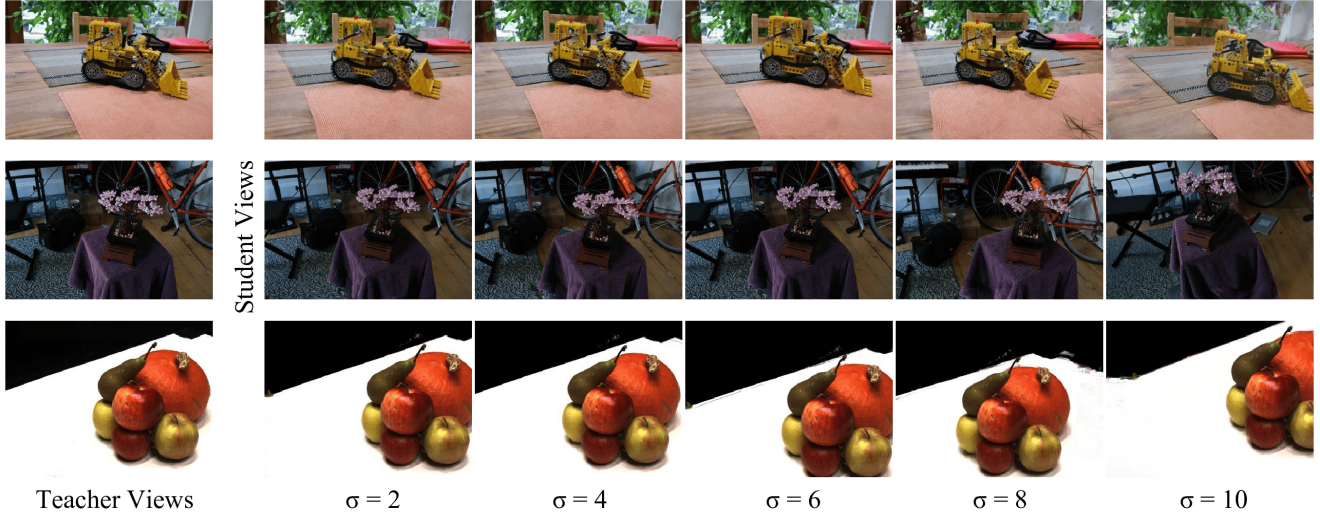


Figure 3. Visualization of student view generation. Examples of pseudo-camera poses with different perturbation magnitudes around teacher view.

perturbation levels σ_i drawn from a predefined range depending on the scene scale and sparsity. This hierarchical sampling naturally forms the basis of our curriculum strategy, where views with smaller perturbations are initially emphasized for stability, and those with larger perturbations are progressively unlocked as training proceeds. Fig. 3 illustrates examples of student views generated at different perturbation levels.

Curriculum scheduling. Instead of introducing all student views simultaneously, we adopt a staged curriculum strategy. Training begins with students at small σ , ensuring stability by augmenting the dataset with near-teacher views that preserve local geometry. After a fixed number of iterations, the curriculum unlocks the next perturbation level, and this process continues iteratively until the largest σ is reached, progressively exposing the model to increasingly diverse viewpoints.

We formalize the active perturbation level at iteration t as:

$$\sigma_{\text{active}}(t) = \min(\sigma_{\text{max}}, \sigma_{\text{min}} + k \cdot \lfloor t/T_s \rfloor), \quad (4)$$

where σ_{min} and σ_{max} denote the minimum and maximum angular perturbations, respectively. T_s is the interval iterations after which the next perturbation level is unlocked, and k is the increment step between successive stages.

By controlling the perturbation schedule through $\sigma_{\text{active}}(t)$, the model first consolidates local consistency around ground-truth views before gradually adapting to larger viewpoint variations. This design alleviates overfitting under sparse supervision and ensures a smooth training trajectory from local refinement to global generalization.

3.3. Student View Evaluation and Promotion

After generating student views, we design an evaluation-and-promotion mechanism that assesses their quality during training and selectively integrates the most reliable candidates into the training set. The purpose of this mechanism is to fully exploit the potential of student views, ensuring that only informative and geometrically consistent samples contribute to model learning.

Evaluation during training. At each training iteration, for each teacher view \mathcal{C}_t , one student view $\mathcal{C}_s^{\sigma_{\text{active}}, j} \in \mathcal{P}(\sigma_{\text{active}})$ is randomly sampled from the pool of student views corresponding to the currently active perturbation level σ_{active} . The corresponding rendered image is then compared against the teacher’s reference image through a composite multi-signal metric. This metric is designed to provide an objective evaluation of student views in the absence of ground-truth references, jointly accounting for structural similarity (SSIM) to assess spatial fidelity, perceptual distance (LPIPS) to measure feature-level realism, and a no-reference image-quality measure [1] to capture global perceptual quality. For each $(\mathcal{C}_t, \sigma_i)$ pair, we maintain the best-performing student, defined as the candidate with the lowest evaluation loss up to the current iteration.

In addition to this scoring mechanism, student views are optimized using auxiliary pseudo-losses based on depth-correlation and co-regularization. Unlike the visual scoring, which serves to select among candidate views, these regularizers operate directly on the selected student views to enhance geometric alignment and multi-view consistency. Further details of these regularization terms are provided in

Sec. 3.4.

Promotion to training views. As the curriculum advances to a new perturbation level σ_{next} , the best-performing student view retained from the previous level σ_{prev} for each teacher is subsequently evaluated. If its visual quality score exceeds a predefined threshold, the corresponding student view is then promoted to the official training set as a valid camera pose. In this manner, only high-quality, geometrically consistent pseudo-views are incorporated, gradually expanding the training coverage.

3.4. Optimization Objective

To ensure robust reconstruction that benefits from dataset expansion while maintaining fidelity to the ground truth, we formulate our objective function with three distinct components: (1) a dynamic reconstruction loss computed over the current training set (comprising both original and promoted student views) to drive the primary optimization; (2) an anchor loss specifically enforced on the fixed original ground-truth views to prevent semantic drift; and (3) student-view geometric regularizers including depth-correlation and dual-model consistency to constrain the structure. The total loss $\mathcal{L}_{\text{total}}$ is defined as:

$$\mathcal{L}_{\text{total}} = \mathcal{L}_{\text{train}} + \lambda_{\text{drift}} \mathcal{L}_{\text{anchor}} + \lambda_{\text{reg}} \mathcal{L}_{\text{reg}} \quad (5)$$

Dynamic Training Loss. This term drives the primary optimization of the 3D Gaussian field. It is computed over the current training set $\mathcal{V}_{\text{train}}$, which is dynamically updated throughout the curriculum. Initially, $\mathcal{V}_{\text{train}}$ contains only the sparse input views. As training progresses, high-confidence student views (pseudo-views that pass our quality curriculum) are added to $\mathcal{V}_{\text{train}}$.

$$\mathcal{L}_{\text{train}} = \frac{1}{|\mathcal{B}_{\text{train}}|} \sum_{I \in \mathcal{B}_{\text{train}}} \mathcal{L}_{\text{photo}}(I, \hat{I}) \quad (6)$$

where $\mathcal{B}_{\text{train}}$ is a batch sampled from $\mathcal{V}_{\text{train}}$, and $\mathcal{L}_{\text{photo}}$ combines L1 and D-SSIM loss. This allows the model to continuously learn from the densified view coverage.

Anchor Loss. As the number of synthetic views in $\mathcal{V}_{\text{train}}$ grows, there is a risk that the optimization may drift or overfit to artifacts in the generated data. To prevent this, we enforce a strict consistency constraint on the fixed set of original input views \mathcal{V}_t (the teacher views). This set remains static throughout training and acts as a geometric anchor. To maintain efficiency, we randomly sample one anchor view $I_{\text{anc}} \sim \mathcal{V}_t$ at each iteration:

$$\mathcal{L}_{\text{anchor}} = \mathcal{L}_{\text{photo}}(I_{\text{anc}}, \hat{I}_{\text{anc}}) \quad (7)$$

By explicitly re-visiting the ground truth at every step, we ensure that the geometric optimization remains anchored to

the reliable observations, preventing semantic drift without incurring the computational cost of rendering all original views.

Student Regularization Loss. Since student views are synthetic observations sampled from the curriculum, they lack ground-truth pixel data for direct supervision. Optimizing these views without constraints can lead to hallucinated geometry or floaters. Therefore, we introduce two pseudo-supervision schemes to regularize the structure of student views. The first scheme is based on depth-correlation. Specifically, we leverage a pretrained monocular depth estimation model [27] to extract a proxy depth map D_{proxy} from the rendered student image. This proxy depth is then compared with the metric depth D_{render} directly output by the 3DGS rasterization via the Pearson correlation coefficient, ensuring that the 3DGS geometry structurally aligns with the visual cues without enforcing an erroneous absolute scale:

$$\mathcal{L}_{\text{depth}} = 1 - \frac{\text{Cov}(D_{\text{render}}, D_{\text{proxy}})}{\sigma_{\text{render}} \sigma_{\text{proxy}}} \quad (8)$$

where Cov denotes covariance and σ denotes standard deviation. The second scheme employs a dual-model consistency constraint. Inspired by recent co-regularization strategies [47], we leverage the insight that valid geometry tends to be consistent across independently trained models, whereas artifacts are typically stochastic and variable. Consequently, we maintain two independently initialized models, \mathcal{M}_A and \mathcal{M}_B , and enforce photometric consistency between their renderings of the same student view, encouraging the models to reach a consensus on the underlying scene structure:

$$\mathcal{L}_{\text{co}} = \|I_{\text{render}}^A - I_{\text{render}}^B\|_2^2 \quad (9)$$

The final regularization term is the weighted sum:

$$\mathcal{L}_{\text{reg}} = \lambda_d \mathcal{L}_{\text{depth}} + \lambda_c \mathcal{L}_{\text{co}} \quad (10)$$

4. Experiments

4.1. Datasets

To comprehensively evaluate the robustness and generalization ability of the proposed CuriGS framework, we conduct extensive experiments on three diverse and widely adopted benchmarks: LLFF [19], MipNeRF-360 [4], and DTU [12]. These datasets encompass a variety of challenging scenarios, ranging from controlled object-centric captures to complex unbounded real-world environments. To ensure a strictly fair comparison, all data splits, image resolutions, and preprocessing steps are kept consistent with prior sparse-view studies [14, 23, 47, 49, 50].

Table 1. Quantitative Comparison With State-of-the-Art Methods on the LLFF, MipNeRF-360, and DTU Datasets. CuriGS Achieves the Best or Comparable Results Across PSNR, SSIM, and LPIPS Metrics Under Sparse-View Conditions.

Method	LLFF (3 Views)			MipNeRF-360 (24 Views)			DTU (3 Views)		
	PSNR \uparrow	SSIM \uparrow	LPIPS \downarrow	PSNR \uparrow	SSIM \uparrow	LPIPS \downarrow	PSNR \uparrow	SSIM \uparrow	LPIPS \downarrow
RegNeRF[21]	19.08	0.587	0.336	22.19	0.643	0.335	18.89	0.745	0.190
SparseNeRF[36]	19.86	0.624	0.328	22.85	0.693	0.315	19.55	0.769	0.201
FreeNeRF[43]	19.63	0.612	0.308	22.78	0.689	0.323	19.92	0.787	0.182
3DGS[13]	18.54	0.588	0.272	21.71	0.672	0.248	17.65	0.816	0.146
DNGaussian[14]	19.12	0.591	0.294	18.06	0.423	0.584	18.91	0.790	0.176
FSGS[50]	20.43	0.682	0.248	23.40	0.733	0.238	17.14	0.818	0.162
CoR-GS[47]	20.45	0.712	0.196	23.55	0.727	0.226	19.21	0.853	0.119
DropGaussian[23]	20.76	0.713	0.200	23.66	0.747	0.233	19.31	0.857	0.142
NexusGS[49]	21.00	0.730	0.179	23.86	0.753	0.206	20.21	0.869	0.102
LoopSparseGS[2]	20.85	0.717	0.205	24.09	0.755	0.226	20.68	0.856	0.125
Ours	21.10	0.732	0.193	24.21	0.761	0.202	20.45	0.873	0.129

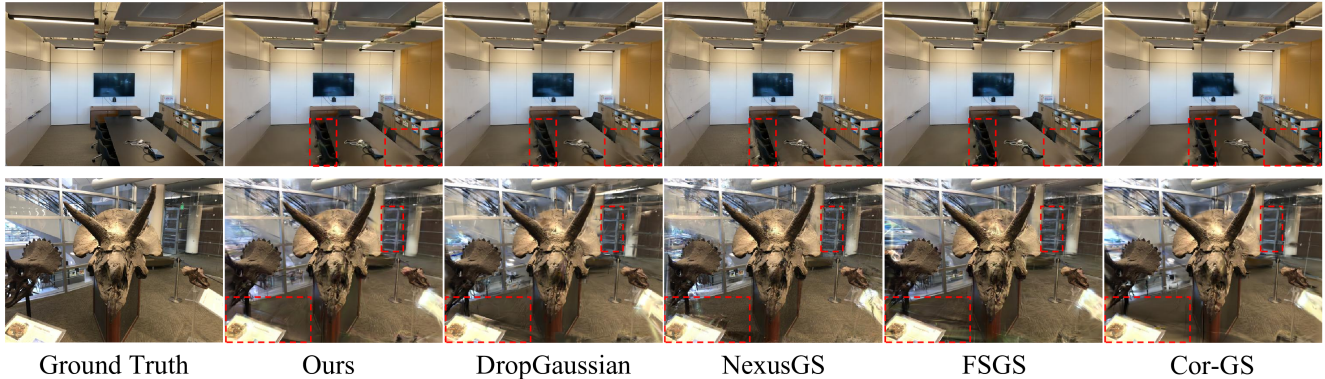


Figure 4. Qualitative comparison on the LLFF dataset. CuriGS achieves sharper details and reduced texture drift compared with other baselines.

LLFF. The LLFF dataset [19] consists of complex, forward-facing real-world scenes captured by handheld cameras. Following the standard evaluation protocol, we designate every 8th image as the test set and utilize the remainder as the training pool. To simulate extreme sparse-view conditions, we uniformly subsample a highly restricted number of views from the training pool to serve as our input. All images are downsampled by a factor of 8 to maintain computational efficiency while aligning with baseline configurations.

MipNeRF-360. The MipNeRF-360 dataset [4] presents highly challenging unbounded indoor and outdoor scenes with intricate background details and 360-degree camera trajectories. This dataset thoroughly tests the model’s capacity to handle scale variations and unbounded backgrounds under sparse supervision. Similar to the LLFF protocol, we reserve every 8th image for testing and uniformly sample a sparse subset from the remaining images for train-

ing. The image resolution is also downsampled by a factor of 8.

DTU. The DTU dataset [12] features object-centric scenes captured under strictly controlled laboratory conditions with precise camera poses. For the DTU dataset, we focus our evaluation on 15 representative scenes, specifically scans 8, 21, 30, 31, 34, 38, 40, 41, 45, 55, 63, 82, 103, 110, and 114. For the extreme sparse-view setting, we specifically utilize views 25, 22, and 28 to construct a 3-view training set, reserving the remaining 25 views for novel view evaluation. All images are downsampled by a factor of 4. Furthermore, to strictly focus the optimization and evaluation on the geometric and photometric fidelity of the target objects, binary masks are applied to isolate and remove the background regions.

4.2. Implementation Details

To handle the varying complexity and scene types across different datasets, we adopt dataset-specific training config-

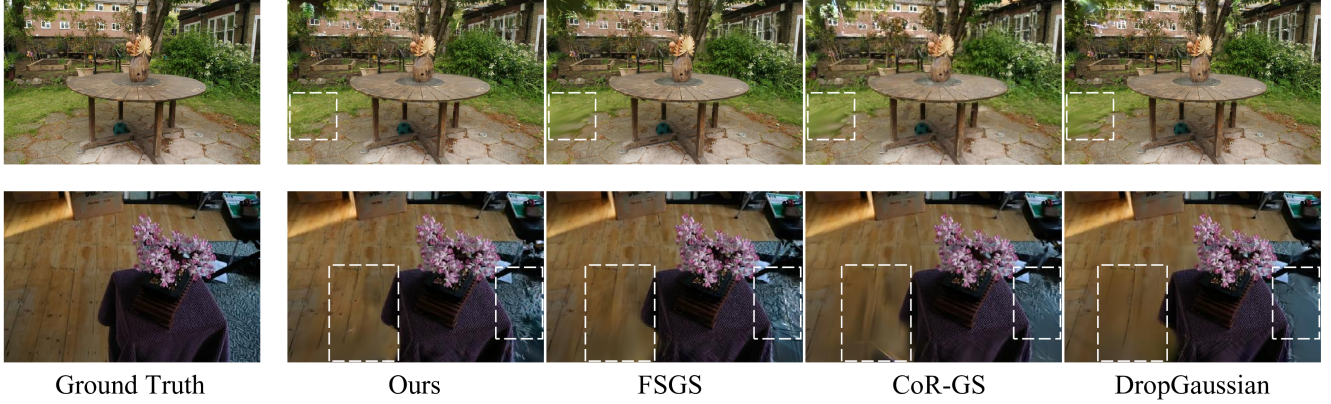


Figure 5. Qualitative comparison on the MipNeRF-360 dataset. CuriGS demonstrates improved perceptual fidelity and geometric stability on large-scale, unbounded scenes.

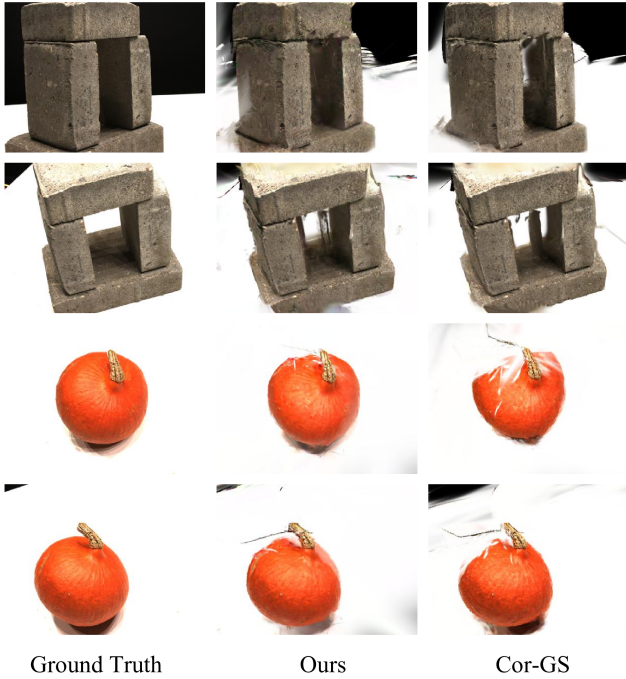


Figure 6. Qualitative comparison on the DTU dataset. CuriGS better preserves fine geometric structures and thin details compared to baseline methods under 3-views sparse supervision.

urations as detailed below.

LLFF. For the LLFF scenes, the model is trained for 30,000 iterations. The curriculum-based student sampling phase is active from iteration 3,000 to 24,000. In this phase, we generate pseudo-student views using perturbation levels $\sigma \in \{1, 2, 3, 4, 5, 6, 7, 8, 9, 10\}$, with 5 students per level. The quality threshold for selecting reliable student views is set to 0.4.

MipNeRF-360. In the MipNeRF-360 dataset, training generally runs for 30,000 iterations, with the curriculum activation scheduled between iterations 7,000 and 27,000. For more complex scenes such as bicycle and stump, we extend the training to 33,000 iterations and the curriculum phase from 10,000 to 30,000. Student views are generated using perturbation levels $\sigma \in \{2, 4, 6, 8, 10\}$, with 3 students per level and a quality threshold of 0.45.

DTU. For the DTU dataset, the model is optimized for 13,000 iterations, with curriculum guidance applied between 2,000 and 12,000 iterations. We utilize perturbation levels $\sigma \in \{1, 2, 3, 4, 5\}$ and sample 10 students per level. The quality threshold is set between 0.45 and 0.55. To maintain object-centric consistency, we apply an adaptive masking strategy for the sampled student views. For a specific student view \mathcal{C}_s , its background mask M_s is determined by the color statistics of the background regions \mathcal{B}_t from its corresponding teacher view \mathcal{C}_t . Let μ_s and σ_s be the mean and standard deviation of pixel colors in \mathcal{C}_s at coordinates corresponding to \mathcal{B}_t . A pixel p in the student view is classified as background if:

$$M_s(p) = \begin{cases} 1, & \text{if } \|\mathcal{C}_s(p) - \mu_s\| < \tau \sigma_s, \\ 0, & \text{otherwise,} \end{cases} \quad (11)$$

where τ is a tolerance threshold. This mechanism ensures that the optimization remains focused on the target object by robustly suppressing background noise, even when geometric perturbations are introduced during the student camera sampling process.

4.3. Baselines

We compared our approach with a representative set of state-of-the-art methods from two categories, including

NeRF-based approaches [21, 36, 43] and recent 3DGS-based methods [14, 23, 47, 49, 50]. For quantitative evaluation, we reported the standard image space metrics PSNR, SSIM, and LPIPS computed on held-out test views.

4.4. Quantitative and Qualitative Results

LLFF. On forward-facing real-world scenes from the LLFF, CuriGS achieves notable gains in both pixel and perceptual level metrics, as shown in Tab. 1. In particular, CuriGS attains the highest PSNR (21.10 dB) and SSIM (0.732) among all compared 3DGS variants, while achieving LPIPS performance competitive with the top baselines. These quantitative improvements correspond to a consistent reduction in cross-view texture drift and localized blurring in visual comparisons (Fig. 4). CuriGS recovers sharper high-frequency appearance around edges and small structures where other methods typically smear or misalign texture. The improvement indicates that selective promotion of high-quality pseudo-views effectively supplements supervision around original camera viewpoints, stabilizing both photometric and geometric reconstruction on challenging forward-facing scenes.

Mip-NeRF360. For large-scale, unbounded scenes from the MipNeRF-360, CuriGS demonstrates robust perceptual quality and strong generalization. Quantitatively, it achieves the best results among the tested methods, with a PSNR of 24.21 dB, SSIM of 0.761, and LPIPS of 0.202 (Tab. 1). The corresponding visual comparisons are shown in Fig. 5. Compared to other baselines, CuriGS exhibits reduced unnatural color shifts and more accurately reconstructs fine details, such as grass and ground textures. These improvements stem from the curriculum strategy, which progressively exposes the model to larger perturbations, while the promotion mechanism filters out inconsistent pseudo-views, ultimately yielding more coherent long-range geometry and perceptually plausible renderings in large-scale scenes.

DTU. On the object-centric DTU benchmark under a 3-views sparse setup, CuriGS shows clear advantages in geometry-sensitive metrics, achieving the highest SSIM, along with competitive PSNR and LPIPS, as shown in Tab. 1. Qualitative comparisons in Fig. 6 further highlight that CuriGS better preserves the overall structural integrity of objects while more effectively maintaining thin structures and fine geometric details, such as small protrusions and edges, which are often lost or distorted by other methods.

4.5. Ablation Study

To better quantify and validate the effectiveness of the proposed CuriGS framework in sparse-view reconstruction, we conduct a comprehensive ablation study.

Table 2. Ablation study on the effect of curriculum guidance.

Dataset	#Views / Setting	PSNR	SSIM	LPIPS
LLFF	2 / Full	20.94	0.768	0.194
	2 / w/o Cur.	18.30	0.601	0.231
	3 / Full	22.51	0.834	0.150
	3 / w/o Cur.	21.03	0.772	0.202
	5 / Full	23.95	0.861	0.140
MipNeRF-360	5 / w/o Cur.	22.97	0.841	0.143
	16 / Full	21.23	0.781	0.189
	16 / w/o Cur.	20.32	0.754	0.202
	24 / Full	23.43	0.851	0.131
DTU	24 / w/o Cur.	22.91	0.830	0.142
	2 / Full	18.66	0.922	0.077
	2 / w/o Cur.	15.04	0.896	0.092
	3 / Full	22.65	0.947	0.050
	3 / w/o Cur.	18.46	0.922	0.065
	6 / Full	24.45	0.947	0.043
	6 / w/o Cur.	20.51	0.946	0.048

Effectiveness of Curriculum Guidance. The overall impact of curriculum guidance across varying datasets and view numbers is demonstrated through consistent and significant improvements in PSNR, SSIM, and LPIPS under diverse sparse-view configurations, as reported in Tab. 2. On the LLFF dataset, curriculum guidance consistently improves performance under all sparse-view conditions. When trained with only two input views, the full strategy achieved a PSNR of 20.94 dB compared to 18.30 dB without guidance, alongside notable increases in SSIM (0.768 vs. 0.601) and decreases in LPIPS (0.194 vs. 0.231). As the number of views increased, overall performance improved, but the model without curriculum guidance still lagged behind.

A similar pattern was observed on the MipNeRF-360 dataset. With 16 views, the inclusion of curriculum guidance improved PSNR from 20.32 dB to 21.23 dB and SSIM from 0.754 to 0.781, while LPIPS decreased from 0.202 to 0.189. At 24 views, the improvements remained consistent, indicating that the proposed mechanism maintains strong generalization capability even as the complexity of the scene increases.

The improvements were even more pronounced on the DTU dataset, which contains structured indoor objects with rich geometric details. The full strategy yielded 3.5–4 dB higher PSNR compared with the baseline lacking curriculum guidance. For example, at three training views, PSNR increased from 18.46 to 22.65, SSIM improved from 0.922 to 0.947, and LPIPS dropped from 0.065 to 0.050.

Effectiveness of Loss Components. To specifically address the structural integrity of our optimization process, we ablate the core loss components formulated in our method:

Table 3. Ablation study on the contribution of each loss component across the LLFF, MipNeRF-360, and DTU datasets.

Dataset	Setting (N)	PSNR \uparrow	SSIM \uparrow	LPIPS \downarrow
LLFF	3 / Full	22.51	0.834	0.150
	3 / w/o Anchor Loss	21.84	0.795	0.178
	3 / w/o Student Reg.	21.48	0.782	0.190
M-360	16 / Full	21.23	0.781	0.189
	16 / w/o Anchor Loss	20.88	0.768	0.194
	16 / w/o Student Reg.	20.65	0.760	0.198
DTU	3 / Full	22.65	0.947	0.050
	3 / w/o Anchor Loss	21.97	0.935	0.058
	3 / w/o Student Reg.	20.82	0.929	0.061

the dynamic reconstruction loss, the anchor loss, and the student-view regularization. First, removing the anchor loss on original views leads to noticeable geometric drift and a drop in overall PSNR, demonstrating its critical role in anchoring the foundational 3D structure against perturbations. Second, excluding the student-view regularization results in the model severely overfitting to the sparse inputs, as it fails to penalize inconsistent geometric priors introduced by unconstrained pseudo-views. Finally, the full triple-loss structure ensures that the dynamic reconstruction leverages the progressive perturbations effectively while maintaining strict fidelity to the ground-truth observations, yielding the most photorealistic and geometrically stable novel-view synthesis.

4.6. Analysis of Pseudo-View Selection Mechanism

In extreme sparse-view scenarios, the fundamental bottleneck lies in the severe lack of multi-view supervision. While expanding the training set via curriculum-guided pseudo-views can mitigate this issue, the unchecked inclusion of poorly rendered views inevitably degrades the underlying geometric fidelity. Therefore, a critical challenge is establishing a robust and dynamic criterion to efficiently evaluate and select high-quality student candidates.

To bridge the supervision gap caused by the absence of explicit ground truth for pseudo-views, we formulate a composite evaluation metric during the continuous tracking phase. This metric elegantly integrates full-reference metrics (LPIPS and SSIM) with a no-reference image-quality score. Specifically, LPIPS and SSIM measure the structural and perceptual deviations from the corresponding teacher view, ensuring that the student maintains strict semantic consistency with the known observations. Simultaneously, the no-reference score penalizes synthetic rendering artifacts, guaranteeing overall image plausibility. Empirically, this tripartite criterion serves as a stable proxy for supervision, effectively screening out degraded viewpoints during the early optimization stages.

Crucially, our strategy adaptively shifts when the train-

ing reaches a perturbation-switching stage. During the final evaluation to promote a student into the permanent training pool, we deliberately decouple the criteria by relying solely on the no-reference quality score. The rationale behind this design is that heavily weighting LPIPS and SSIM at the promotion stage inherently biases the selection toward students spatially closest to the teacher, thereby stifling viewpoint diversity. By tolerating moderate geometric or appearance deviations—provided the standalone rendering quality remains high—the model is compelled to explore broader scene variations. As visualized in Fig. 7, this dynamic selection mechanism not only progressively refines the student renders but also successfully identifies the optimal candidate that balances structural coherence with informative viewpoint expansion, ultimately enhancing the generalization and robustness of the 3D representation.

4.7. Analysis of Training Dynamics

To further investigate the dynamic impact of our curriculum-guided expansion, we monitor the evolution of PSNR, SSIM, and LPIPS metrics throughout the training process on a representative DTU scene. As depicted in Fig. 8, the baseline without curriculum guidance exhibits a distinctive performance decay in the later stages of optimization—a hallmark of overfitting where the model memorizes sparse training viewpoints at the expense of general scene structure. In contrast, CuriGS maintains a steady and upward trajectory across all evaluation metrics. This sustained improvement demonstrates that the progressive integration of validated student views provides a continuous and reliable supervisory signal, effectively anchoring the optimization process and ensuring consistent convergence toward a high-fidelity representation.

5. Conclusion

In this work, we present CuriGS, a curriculum-guided framework for sparse view 3D reconstruction using 3DGS. Our method tackles the core challenge of sparse supervision by introducing a hierarchical student-view learning mechanism, in which pseudo-views are progressively sampled and regularized according to a curriculum schedule. By leveraging multi-signal evaluation metrics that combine perceptual, structural, and image-quality measures, CuriGS selectively promotes high-quality student views, thereby enhancing geometric consistency and photometric fidelity. Extensive experiments on the LLFF, MipNeRF-360, and DTU datasets demonstrate that CuriGS consistently outperforms existing NeRF- and 3DGS-based baselines under various sparse-view settings. The curriculum-guided strategy substantially mitigates overfitting, improves generalization to unseen viewpoints, and preserves fine geometric details even under extreme sparsity.

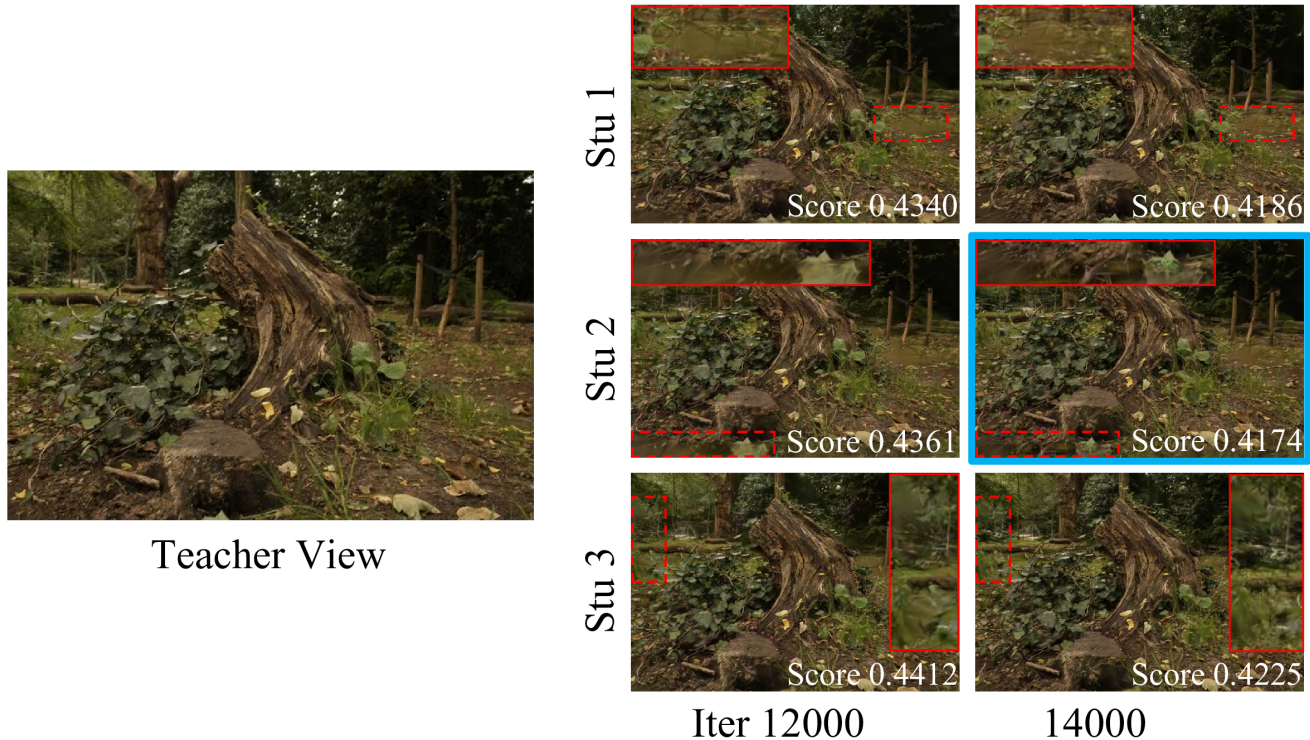


Figure 7. Visualization of a teacher view and its associated student-view group under a specific perturbation magnitude. From left to right, the rendered results of the students are shown across different training stages, illustrating the progressive enhancement of visual fidelity and structural coherence. The composite evaluation scores (where lower indicates better quality) are utilized to track performance, with the optimal student candidate highlighted by a blue box.

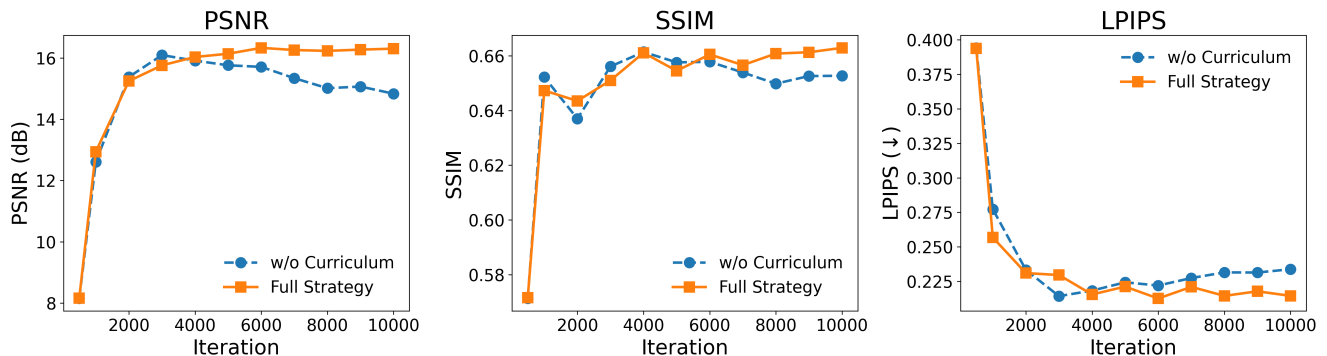


Figure 8. Evolution of PSNR, SSIM, and LPIPS during training on a DTU scene with and without curriculum guidance.

References

- [1] Lorenzo Agnolucci, Leonardo Galteri, and Marco Bertini. Quality-aware image-text alignment for opinion-unaware image quality assessment. *arXiv preprint arXiv:2403.11176*, 2024. 2, 5
- [2] Zhenyu Bao, Guibiao Liao, Kaichen Zhou, Kanglin Liu, Qing Li, and Guoping Qiu. Loopsparsegs: Loop based sparse-view friendly gaussian splatting. *IEEE Transactions on Image Processing*, 2025. 2, 3, 7
- [3] Jonathan T Barron, Ben Mildenhall, Matthew Tancik, Peter Hedman, Ricardo Martin-Brualla, and Pratul P Srinivasan. Mip-nerf: A multiscale representation for anti-aliasing neural radiance fields. In *Proceedings of the IEEE/CVF international conference on computer vision*, pages 5855–5864, 2021. 1
- [4] Jonathan T Barron, Ben Mildenhall, Dor Verbin, Pratul P Srinivasan, and Peter Hedman. Mip-nerf 360: Unbounded anti-aliased neural radiance fields. In *Proceedings of the IEEE/CVF conference on computer vision and pattern*

- recognition, pages 5470–5479, 2022. 6, 7
- [5] Yuanhao Cai, Jiahao Wang, Alan Yuille, Zongwei Zhou, and Angtian Wang. Structure-aware sparse-view x-ray 3d reconstruction. In *Proceedings of the IEEE/CVF conference on computer vision and pattern recognition*, pages 11174–11183, 2024. 1
- [6] David Charatan, Sizhe Lester Li, Andrea Tagliasacchi, and Vincent Sitzmann. pixelsplat: 3d gaussian splats from image pairs for scalable generalizable 3d reconstruction. In *Proceedings of the IEEE/CVF conference on computer vision and pattern recognition*, pages 19457–19467, 2024. 1
- [7] Anpei Chen, Zexiang Xu, Fuqiang Zhao, Xiaoshuai Zhang, Fanbo Xiang, Jingyi Yu, and Hao Su. Mvsnerf: Fast generalizable radiance field reconstruction from multi-view stereo. In *Proceedings of the IEEE/CVF international conference on computer vision*, pages 14124–14133, 2021. 1
- [8] Zhien Dai, Zhaohui Tang, Hu Zhang, and Yongfang Xie. Mgs-stereo: Multi-scale geometric-structure-enhanced stereo matching for complex real-world scenes. *IEEE Transactions on Image Processing*, 34:6246–6258, 2025. 1
- [9] Kangle Deng, Andrew Liu, Jun-Yan Zhu, and Deva Ramanan. Depth-supervised nerf: Fewer views and faster training for free. In *Proceedings of the IEEE/CVF conference on computer vision and pattern recognition*, pages 12882–12891, 2022. 2
- [10] Liang Han, Junsheng Zhou, Yu-Shen Liu, and Zhizhong Han. Binocular-guided 3d gaussian splatting with view consistency for sparse view synthesis. *Advances in Neural Information Processing Systems*, 37:68595–68621, 2024. 1
- [11] Ajay Jain, Matthew Tancik, and Pieter Abbeel. Putting nerf on a diet: Semantically consistent few-shot view synthesis. In *Proceedings of the IEEE/CVF international conference on computer vision*, pages 5885–5894, 2021. 2
- [12] Rasmus Jensen, Anders Dahl, George Vogiatzis, Engin Tola, and Henrik Aanæs. Large scale multi-view stereopsis evaluation. In *Proceedings of the IEEE conference on computer vision and pattern recognition*, pages 406–413, 2014. 6, 7
- [13] Bernhard Kerbl, Georgios Kopanas, Thomas Leimkühler, and George Drettakis. 3d gaussian splatting for real-time radiance field rendering. *ACM Trans. Graph.*, 42(4):139–1, 2023. 1, 7
- [14] Jiahe Li, Jiawei Zhang, Xiao Bai, Jin Zheng, Xin Ning, Jun Zhou, and Lin Gu. Dngaussian: Optimizing sparse-view 3d gaussian radiance fields with global-local depth normalization. In *Proceedings of the IEEE/CVF conference on computer vision and pattern recognition*, pages 20775–20785, 2024. 2, 3, 6, 7, 9
- [15] Ming Liu, Yuxuan Liang, Siwei Chen, Junjie Wang, and Yang Na. Sv-2dgs: Optimization of sparse view 3d reconstruction based on 2dgs models. *Expert Systems with Applications*, 297:129334, 2026. 3
- [16] Yang Liu, Chuanchen Luo, Lue Fan, Naiyan Wang, Junran Peng, and Zhaoxiang Zhang. Citygaussian: Real-time high-quality large-scale scene rendering with gaussians. In *European Conference on Computer Vision*, pages 265–282. Springer, 2024. 1
- [17] Xiaoxiao Long, Cheng Lin, Peng Wang, Taku Komura, and Wenping Wang. Sparseneus: Fast generalizable neural surface reconstruction from sparse views. In *European Conference on Computer Vision*, pages 210–227. Springer, 2022. 1
- [18] Saswat Subhajyoti Mallick, Rahul Goel, Bernhard Kerbl, Markus Steinberger, Francisco Vicente Carrasco, and Fernando De La Torre. Taming 3dgs: High-quality radiance fields with limited resources. In *SIGGRAPH Asia 2024 Conference Papers*, pages 1–11, 2024. 1
- [19] Ben Mildenhall, Pratul P Srinivasan, Rodrigo Ortiz-Cayon, Nima Khademi Kalantari, Ravi Ramamoorthi, Ren Ng, and Abhishek Kar. Local light field fusion: Practical view synthesis with prescriptive sampling guidelines. *ACM Transactions on Graphics (ToG)*, 38(4):1–14, 2019. 6, 7
- [20] Ben Mildenhall, Pratul P Srinivasan, Matthew Tancik, Jonathan T Barron, Ravi Ramamoorthi, and Ren Ng. Nerf: Representing scenes as neural radiance fields for view synthesis. *Communications of the ACM*, 65(1):99–106, 2021. 1
- [21] Michael Niemeyer, Jonathan T Barron, Ben Mildenhall, Mehdi SM Sajjadi, Andreas Geiger, and Noha Radwan. Regnerf: Regularizing neural radiance fields for view synthesis from sparse inputs. In *Proceedings of the IEEE/CVF conference on computer vision and pattern recognition*, pages 5480–5490, 2022. 2, 7, 9
- [22] Avinash Paliwal, Wei Ye, Jinhui Xiong, Dmytro Kotovenko, Rakesh Ranjan, Vikas Chandra, and Nima Khademi Kalantari. Coherentgs: Sparse novel view synthesis with coherent 3d gaussians. In *European Conference on Computer Vision*, pages 19–37. Springer, 2024. 3
- [23] Hyunwoo Park, Gun Ryu, and Wonjun Kim. Dropgaussian: Structural regularization for sparse-view gaussian splatting. In *Proceedings of the Computer Vision and Pattern Recognition Conference*, pages 21600–21609, 2025. 3, 6, 7, 9
- [24] Albert Pumarola, Enric Corona, Gerard Pons-Moll, and Francesc Moreno-Noguer. D-nerf: Neural radiance fields for dynamic scenes. In *Proceedings of the IEEE/CVF conference on computer vision and pattern recognition*, pages 10318–10327, 2021. 1
- [25] Charles R Qi, Hao Su, Kaichun Mo, and Leonidas J Guibas. Pointnet: Deep learning on point sets for 3d classification and segmentation. In *Proceedings of the IEEE conference on computer vision and pattern recognition*, pages 652–660, 2017. 1
- [26] Zhiyin Qian, Shaofei Wang, Marko Mihajlovic, Andreas Geiger, and Siyu Tang. 3dgs-avatar: Animatable avatars via deformable 3d gaussian splatting. In *Proceedings of the IEEE/CVF conference on computer vision and pattern recognition*, pages 5020–5030, 2024. 1
- [27] René Ranftl, Alexey Bochkovskiy, and Vladlen Koltun. Vision transformers for dense prediction. In *Proceedings of the IEEE/CVF international conference on computer vision*, pages 12179–12188, 2021. 6
- [28] Johannes L Schonberger and Jan-Michael Frahm. Structure-from-motion revisited. In *Proceedings of the IEEE conference on computer vision and pattern recognition*, pages 4104–4113, 2016. 1

- [29] Maria Skublewska-Paszowska, Marek Milosz, Pawel Powroznik, and Edyta Lukasik. 3d technologies for intangible cultural heritage preservation—literature review for selected databases. *Heritage Science*, 10(1):3, 2022. 1
- [30] Nagabhushan Somraj and Rajiv Soundararajan. Vip-nerf: Visibility prior for sparse input neural radiance fields. In *ACM SIGGRAPH 2023 conference proceedings*, pages 1–11, 2023. 1, 2
- [31] Nagabhushan Somraj, Sai Harsha Mupparaju, Adithyan Karanayil, and Rajiv Soundararajan. Simple-rf: Regularizing sparse input radiance fields with simpler solutions. *arXiv preprint arXiv:2404.19015*, 2024. 2
- [32] Stanislaw Szymanowicz, Christian Rupprecht, and Andrea Vedaldi. Splatter image: Ultra-fast single-view 3d reconstruction. In *Proceedings of the IEEE/CVF conference on computer vision and pattern recognition*, pages 10208–10217, 2024. 1
- [33] Yutao Tang, Yuxiang Guo, Deming Li, and Cheng Peng. Spars3r: Semantic prior alignment and regularization for sparse 3d reconstruction. In *Proceedings of the Computer Vision and Pattern Recognition Conference*, pages 26810–26821, 2025. 3
- [34] Fei Tao, Bin Xiao, Qinglin Qi, Jiangfeng Cheng, and Ping Ji. Digital twin modeling. *Journal of Manufacturing Systems*, 64:372–389, 2022. 1
- [35] Yecong Wan, Mingwen Shao, Yuanshuo Cheng, and Wangmeng Zuo. S2gaussian: Sparse-view super-resolution 3d gaussian splatting. In *Proceedings of the Computer Vision and Pattern Recognition Conference*, pages 711–721, 2025. 3
- [36] Guangcong Wang, Zhaoxi Chen, Chen Change Loy, and Ziwei Liu. Sparsenerf: Distilling depth ranking for few-shot novel view synthesis. In *Proceedings of the IEEE/CVF international conference on computer vision*, pages 9065–9076, 2023. 1, 2, 7, 9
- [37] Kangkan Wang, Chong Wang, Jian Yang, and Guofeng Zhang. Clocap-gs: Clothed human performance capture with 3d gaussian splatting. *IEEE Transactions on Image Processing*, 34:5200–5214, 2025. 1
- [38] Nanyang Wang, Yinda Zhang, Zhuwen Li, Yanwei Fu, Wei Liu, and Yu-Gang Jiang. Pixel2mesh: Generating 3d mesh models from single rgb images. In *Proceedings of the European conference on computer vision (ECCV)*, pages 52–67, 2018. 1
- [39] Yuxuan Wang, Xuanyu Yi, Zike Wu, Na Zhao, Long Chen, and Hanwang Zhang. View-consistent 3d editing with gaussian splatting. In *European conference on computer vision*, pages 404–420. Springer, 2024. 1
- [40] Yu Wang, Xiaobao Wei, Ming Lu, and Guoliang Kang. Plgs: Robust panoptic lifting with 3d gaussian splatting. *IEEE Transactions on Image Processing*, 34:3377–3388, 2025. 1
- [41] Haolin Xiong, Sairisheek Muttukuru, Hanyuan Xiao, Rishi Upadhyay, Pradyumna Chari, Yajie Zhao, and Achuta Kadambi. Sparsegs: Sparse view synthesis using 3d gaussian splatting. In *2025 International Conference on 3D Vision (3DV)*, pages 1032–1041. IEEE, 2025. 3
- [42] Yinghao Xu, Zifan Shi, Wang Yifan, Hansheng Chen, Ceyuan Yang, Sida Peng, Yujun Shen, and Gordon Wetstein. Grm: Large gaussian reconstruction model for efficient 3d reconstruction and generation. In *European Conference on Computer Vision*, pages 1–20. Springer, 2024. 1
- [43] Jiawei Yang, Marco Pavone, and Yue Wang. Freenerf: Improving few-shot neural rendering with free frequency regularization. In *Proceedings of the IEEE/CVF conference on computer vision and pattern recognition*, pages 8254–8263, 2023. 1, 2, 7, 9
- [44] Alex Yu, Vickie Ye, Matthew Tancik, and Angjoo Kanazawa. pixelnerf: Neural radiance fields from one or few images. In *Proceedings of the IEEE/CVF conference on computer vision and pattern recognition*, pages 4578–4587, 2021. 2
- [45] Shuwan Yu, Xiaolang Liu, Qianqiu Tan, Zitong Wang, and Baohua Zhang. Sensors, systems and algorithms of 3d reconstruction for smart agriculture and precision farming: A review. *Computers and Electronics in Agriculture*, 224:109229, 2024. 1
- [46] Daiwei Zhang, Joaquin Gajardo, Tomislav Medic, Isinsu Katircioglu, Mike Boss, Norbert Kirchgessner, Achim Walter, and Lukas Roth. Wheat3dgs: In-field 3d reconstruction, instance segmentation and phenotyping of wheat heads with gaussian splatting. In *Proceedings of the Computer Vision and Pattern Recognition Conference*, pages 5360–5370, 2025. 1
- [47] Jiawei Zhang, Jiahe Li, Xiaohan Yu, Lei Huang, Lin Gu, Jin Zheng, and Xiao Bai. Cor-gs: sparse-view 3d gaussian splatting via co-regularization. In *European Conference on Computer Vision*, pages 335–352. Springer, 2024. 3, 6, 7, 9
- [48] Yao Zhang, Jiangshu Wei, Yuchao Wang, and Jiajun Liu. UsGs: Enhancing sparse view synthesis with unseen viewpoint regularization in 3d gaussian splatting. *Pattern Recognition*, 170:112087, 2026.
- [49] Yulong Zheng, Zicheng Jiang, Shengfeng He, Yandu Sun, Junyu Dong, Huaidong Zhang, and Yong Du. Nexusgs: Sparse view synthesis with epipolar depth priors in 3d gaussian splatting. In *Proceedings of the Computer Vision and Pattern Recognition Conference*, pages 26800–26809, 2025. 3, 6, 7, 9
- [50] Zehao Zhu, Zhiwen Fan, Yifan Jiang, and Zhangyang Wang. Fsgs: Real-time few-shot view synthesis using gaussian splatting. In *European conference on computer vision*, pages 145–163. Springer, 2024. 2, 3, 6, 7, 9